High activated carbon loading mixed matrix membranes for gas separations

M. G. García, J. Marchese & N. A. Ochoa

Journal of Materials Science
Full Set - Includes `Journal of Materials Science Letters'

ISSN 0022-2461
Volume 47
Number 7

J Mater Sci (2012) 47:3064-3075
DOI 10.1007/s10853-011-6138-8

Springer

J Mater Sci (2012) 47:3064–3075
DOI 10.1007/s10853-011-6138-8

High activated carbon loading mixed matrix membranes for gas separations

M. G. García · J. Marchese · N. A. Ochoa

Received: 6 October 2011 / Accepted: 15 November 2011 / Published online: 29 November 2011

Abstract Mixed matrix membranes (MMMs) containing highest amounts of activated carbon (AC) reported to date were prepared for gas separation. A polymeric phase of semicrystalline polyvinyl chloride (PVC) was loaded with different amounts (from 23 to 60 wt%) of AC, and then was crosslinked using an aromatic diamine. Thermal treatment was used to complete the crosslinking reaction. Uncrosslinked MMMs were also prepared. FT-IR, SEM microscopy, X-ray diffraction, thermal degradation, and differential scanning calorimetry characterization techniques were used to verify the extent of crosslinking, crystalline structure, and the thermal resistance of the membranes. Crosslinked PVC membrane has higher both permeation flux and selectivity than the uncrosslinked one. It was observed the crosslinking process favored the formation of a less permeable porous structure in all MMMs. A decrease in the polymer crystallinity as the carbon content increased was also observed. This effect was more pronounced in absent of crosslinking. Crosslinked MMMs showed higher thermal resistance than uncrosslinked ones and pure PVC. Permeation tests showed crosslinked MMMs were more selective; i.e., the gas pair H_2/CH_4 selectivities varied from diffusion to Knudsen mechanisms (α_{H_2/CH_4} 11.87–2.25), whereas the selectivity of uncrosslinked MMMs varied from Knudsen to viscous mechanisms (α_{H_2/CH_4} 2.42–1.89). High AC content MMMs possessed permeability values comparable to those of pyrolytic carbon membranes.

M. G. García · J. Marchese · N. A. Ochoa (✉)
Instituto de Física Aplicada-INFAP, Universidad Nacional de San Luis-CONICET-FONCYT, Chacabuco, San Luis 917-5700, Argentina
e-mail: aochoa@unsl.edu.ar

Introduction

Membrane processes for gas separation have improved remarkably over the past few decades. Significant effort has been focused on the synthesis of gas separation membranes based on materials that provide better selectivity, and thermal and chemical stability, than those already in use, such as polymeric membranes. In fact, non-polymeric and inorganic membranes have attracted considerable attention in recent years, particularly in studies attempting to improve the performance of membrane materials for gas separations [1].

Of the currently available non-polymeric membranes, molecular sieving materials, such as silica, zeolites, and carbon, have the potential to extend the upper boundary of the permeability versus selectivity trade-off [2–5]. In fact, because of their unique microporous structure, which can discriminate gas molecules by size and shape, zeolitic materials and carbon molecular sieves have been used as adsorbents and catalysts in many adsorptive separations and catalytic processes. Moreover, by incorporating zeolites and carbon molecular sieves into polymers, to form mixed matrix membranes (MMMs), much greater size and shape selectivity can be achieved [6–10]. However, the rigid nature of molecular sieves makes the formation of continuous and defect-free membranes difficult, especially for glassy polymers. Furthermore, poor particle adhesion and phase separation are common problems with MMMs, which greatly limit their application [11]. To address some of these issues, several research groups have attempted to improve the particle–polymer interfacial adhesion [12].

For example, both Mahajan and Koros [13], and Marchese et al. [14, 15], found that more flexible polymers, and glassy polymers with flexible segments in their

backbone, enable the introduction of increased amounts of inorganic filler than conventional MMMs, and improve membrane selectivity at the particle–polymer interfacial region.

Although porous inorganic membranes were first developed before 1945, they were not widely recognized until high quality porous ceramic membranes became available for industrial usage on a large scale [16, 17]. Nowadays, inorganic membranes are used primarily for energy-related applications. They have become important tools for beverage production, water purification, and the separation of dairy products. In addition, they play a significant role in the industrial gas separation processes [16]. Carbon membranes are one of the most attractive inorganic membranes for gas separation processes [18], and have several advantages over other membranes, including: higher permselectivity than any known polymer membrane; superior stability at high temperatures; thermochemically adjustable pore dimensions and size distributions; and superior adsorptivity for certain specific gases. Carbon membranes are formed via pyrolysis of polymeric precursors. The key factors that determine the transport properties of resultant carbon membranes include: the chemical structure of the polymer precursor, and the pyrolysis process parameters used during synthesis. However, in spite of their advantages, carbon membranes are very brittle, and require careful handling and repeated pre- and post-treatments to maintain performance [18]. Some of these difficulties may be partially alleviated by optimizing the polymer precursors and preparation methods [19]. Barrer et al. [20] reported the successful preparation of carbon membranes by carbonization of suitable carbon-containing materials under an inert atmosphere or vacuum. The resulting carbonaceous material was compressed into a plug to obtain porous or non-porous carbon membranes. Subsequently, many researchers, such as Fuertes [21], reported preparation of carbon membranes by deposition of a thin film of phenolic resin or polymeric solution on the inner face of a macroporous support, such as alumina, followed by application of the pyrolysis process. Based on these studies, the thickness of the microporous carbon layer was found to be an important factor in this preparation method. Other researchers applied a coating technique to repair defects in carbon membranes. For example, Petersen et al. [22] treated a carbonized membrane with a thin layer of polydimethylsiloxane (PDMS) to prevent gas flux through defect structures. Specifically, the membrane was immersed in a 2% solution of PDMS (WACKER E41) in heptane, and then withdrawn to harden the coated layer.

In 2004 Ismail and Saufi [1] reviewed the fabrication of carbon membranes, and showed that the synthesis of carbon membranes requires several steps and experimental handling. In addition, although carbon membranes for gas separation have been studied in terms of preparation and application, the mechanism of gas transport through the membrane is not well known. It is believed that gas transport in porous carbon membranes can occur via several mechanisms: Knudsen diffusion; surface diffusion; capillary condensation; molecular sieving; and viscous flux. The first four of these mechanisms can be exploited for the separation of gas mixtures. The main mechanism can be determined through permeation experiments [19].

In the present work, high carbon content MMMs (HCMMMs) were prepared from a soft polymer and a commercial activated carbon (AC) for use in gas separation. An alternative method of obtaining highly permeable membranes with good processability is proposed. The HCMMMs consisted of a semicrystalline polymer loaded with different amounts of AC (up to 60 wt%). The influence of AC load and crosslinking agent on the polymeric matrix was studied and the gas transport mechanism in the resulting MMMs was analysed. HCMMMs were also characterized using FT-IR analysis, SEM imaging, X-ray diffraction spectroscopy, thermal degradation (TG), differential scanning calorimetry (DSC), and gas permeation.

Experimental

Materials and methods

Soft polyvinyl chloride (PVC, Sigma) was used as continuous phase of MMMs. Soft PVC (density = 1.214 g cm^{-3}) is obtained by mixing rigid PVC with a plasticizer (bis-(2-ethylhexyl)phthalate (DEHP)) to improve some of the properties of the material, especially in terms of processability and flexibility. Distinct advantages arising from PVC plasticization are low cost, versatile processing of various shapes and designs [23], which make soft PVC the main alternative to replace flexible products based on elastomers or leather. The main limitations in the application of soft PVC come from its poor thermal and chemical resistance properties [24, 25]. Crosslinking soft PVC by using a crosslinking agent is the most effective way to improve thermal and transport properties of flexible PVC. In this work a difunctional amine 4,4′-oxidianiline (ODA, Sigma), was used as crosslinking agent of the polymeric matrix. ODA is an aromatic diamine with two phenyl rings bound by an ether group. ODA was purified by recrystallization from the ethanol solution. Tetrahydrofuran (THF, Fluka) was used as solvent.

Activated carbon Maxsorb 3000 (AC), a powder with high surface area provided by Kansai Coke & Chemical Co. Ltd. (Japan), was used as inorganic filler of HCMMMs. Marchese et al. [14, 26] reported the structural characteristics of the AC, namely, surface area, *Sw* (m^2/g): 3272; pore size

distribution between 7 and 30 Å; mean pore width size, d_p (Å) 21.7; high porosity, $\varepsilon = 0.87$; density = 0.28 g cm^{-3}; and particle size distribution between 0.2 and 20 μm.

The pure gases used for the permeation study include H_2, N_2, O_2, CH_4 and CO_2. The purity of the pure gases was more than 99.95%. All gases were supplied by air liquid (Argentina).

Preparation of HCMMMs

A polymeric solution of PVC was prepared by dissolving 7% (w/v) soft PVC in THF solvent under continuous stirring with a magnetic bar at 300 rpm for 4 h at 25 °C. Then, 0.05 g ODA was added to an Erlenmeyer flask containing the PVC solution. The mixture was then treated in the flask in an ultrasonic bath for 1 h, followed by mechanical stirring for 1 h. After that, a corresponding amount of AC (23–60 wt%) was gently added to the PVC–ODA solution under mechanical stirring and sonication at ambient temperature (25 °C) for more than 1 h. Sonication and stirring enhance the homogeneous distribution of carbon particles in the polymer solution, decreasing the formation of carbon agglomerates. The obtained suspensions were filtered using a #400 mesh, and cast (at 25 °C in air; relative humidity 45%) using a glass sample support. The resulting MMMs with high AC content were dried under vacuum at 80 °C for 48 h, and then cured at 120 °C for 30 min, followed by 140 °C for 60 min under N_2 atmosphere. The thermal treatment was applied in order to promote the crosslinking reaction. The thicknesses of the resulting HCMMMs were measured with a Köfer micrometer (precision ± 1 μm), and ranged from 60 to 1970 μm. The same preparation method was used to prepare carbon membranes without adding ODA, in order to analyse the effect of crosslinking agent.

HCMMMs characterization

FT-IR analysis

FT-IR spectra were determined by the diffuse reflectance (DRIFTS) mode using a Nicolet PROTEGE 460 Spectrometer and the transmission mode using a Varian 640 Spectrometer. The operational range was 400–4000 cm^{-1}. The number of scans for each sample was 64.

SEM analysis

Electron micrographs were obtained by a scanning electron microscope LEO 1450VP. The HCMMMs were fractured in liquid nitrogen and mounted on sample holder previous coverage with a conductive material. SEM imaging was examined using an accelerating voltage of 15 kV.

X-ray diffraction

Wide angle X-ray diffractions (WAXD) studies were carried out using an equipment Rigaku model D-Max III C, lamp of Cu Kα and filter of Nickel. The 2θ operational range ranged from 0° to 60°. The d-spacing of each HCMMM was determined by Bragg's equation (Eq. 1).

$$n\lambda = 2d \sin\theta \tag{1}$$

where d is the average intercatenary distance, n is the integer determined, λ is the wavelength of the X-ray (nm), and θ is the Bragg's angle.

Thermal analysis (DSC and TGA)

Differential scanning calorimetry and thermogravimetric analysis (TGA) were performed to estimate the glass transition temperature (T_g) and the thermal stability of the membranes. The DSC and TG measurements were recorded on MDSC 2920 and TG 2950 analyzers (TAInstruments, Inc., Newcastle, USA), respectively. The operating conditions were as follows: (a) heating rate: 20° min^{-1} and (b) atmosphere: dynamic N_2 (99.99%, flow rate 50 mL/min). The DSC and TG temperature axes were calibrated with indium (99.99%, mp 156.60 °C) and the Curie point of Ni (353 °C), respectively. Empty aluminum pans (40 μL) were used as references. Samples of ~ 10 mg were employed. The DSC values reported were obtained applying two scans (heating and cooling) over each sample and they result from the average of at least two independent measurements. Data were collected with Thermal Solutions software (TA Instrument, Inc.).

Gas permeation measurements

Permeability was measured using a classical time-lag apparatus [14, 23]. The effective membrane area was 11.34 cm^2 and permeate constant volume was 35.37 cm^3. The amount of gas transmitted at time "t" through the membrane was calculated from the permeate pressure (p_2) readings in the low-pressure side of permeation cell. Permeability coefficients (P_i) were obtained directly from the flux rate into the downstream volume upon reaching the steady state as:

$$P_i = \frac{B\ell}{T_c p_1}\frac{dp_2}{dt} \tag{2}$$

where B is the cell constant = 11.53 (cm^3(STP) K)/(cm^2 cmHg); dp_2/dt (cmHg/s); p_1 is high-pressure side (cmHg); ℓ is membrane thickness (cm); T_c is the cell

temperature (K). Theoretical separation factors ($\alpha_{i/j}$) were calculated as the ratio between the permeation coefficients of pure gases i and j:

$$\alpha_{i/j} = \frac{P_i}{P_j} \tag{3}$$

Results and discussion

FT-IR spectra

Fourier transform infrared spectroscopy (FT-IR) was performed to analyse the mechanisms involved in the PVC crosslinking reaction, by monitoring the evolution of some characteristic infrared absorbance peaks. Furthermore, the influence of AC content in the polymeric matrix was analysed.

PVC characteristic peaks were located at 617–694 cm^{-1}, corresponding to C–Cl bond stretching vibrations, and at 2910 and 2972 cm^{-1}, corresponding to C–H bonds [23, 27, 28]. During diamine crosslinking, the chlorine atom is extracted from the main polymer chain and replaced by a crosslinker moiety (ODA), resulting in a decrease in peak intensity at 694 cm^{-1}. This result was confirmed by the appearance of a broad peak at 3444 cm^{-1}, which was attributed to disubstituted nitrogen, which is formed during the crosslinking process [29]. A comparison of the characteristic FT-IR peaks for pure PVC and crosslinked PVC is shown in Fig. 1.

Additional peaks were observed in the PVC/ODA spectrum at 1498 and 1604–1582 (doublet) cm^{-1}. The peak at 1498 cm^{-1} was attributed to C–N bond stretching vibrations, which confirmed the presence of crosslinking

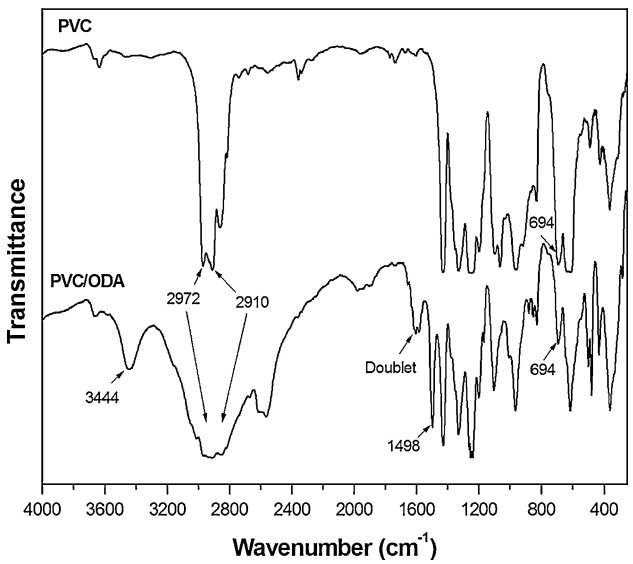

Fig. 1 FT-IR spectra of PVC and PVC/ODA

bonds, and the doublet was attributed to both aromatic double bonds on the crosslinker molecule and the formation of double bonds on the main polymer chain, indicating that some degradation occurred during crosslinking of PVC with difunctional amines. The degradation appears to be the result of side reactions which took place during the crosslinking reaction and the thermal curing process. Using the above-described FT-IR analysis as a guide, a crosslinking mechanism is propose, where each crosslinking reaction involves the loss of two HCl molecules for every molecule of crosslinked amine (see Fig. 2a). As illustrated in Fig. 2b [30], this crosslinking mechanism also explains the degradation of PVC, which could occur by HCl catalyzed dehydrochlorination via an ion pair reaction.

Because of the dark appearance of the membranes, FT-IR spectra of crosslinked and uncrosslinked HCMMMs were acquired using the DRIFTS technique. FT-IR spectra for PVC–23% AC and PVC/ODA–23% AC are shown in Fig. 3. As can be seen, the intensity of the IR band at 694 cm^{-1} decreases for both membranes, indicating that the thermal curing process also promotes the loss of chlorine atoms. This result is in agreement with Romero Tendero et al. [23], who reported that HCl molecules were lost during PVC thermal treatment.

PVC–23% AC and PVC/ODA–23% AC also displayed characteristic C–H stretching bands at 2910–2972 cm^{-1}. However, bands at 3444 and 1498 cm^{-1} were not observed for the PVC/ODA–23% AC membrane, probably because of the diffuse reflectance was unable to penetrate deeply in the sample in presence of the AC particles.

The doublet observed at 1604–1582 cm^{-1} in the PVC/ODA membrane appears to be resolved into two distinct single peaks at 1612 and 1516 cm^{-1} in FT-IR spectra of the PVC/ODA–23% AC membrane. Both signals were attributed to double bonds formed during the crosslinking reaction and subsequent thermal treatment. These same bands appeared at higher wavenumbers (1618 and 1518 cm^{-1}) in the PVC–23% AC membrane, indicating that double bonds in crosslinked HCMMMs may take part in resonant structures with double bonds and nitrogen atoms from the diamine molecules.

FT-IR spectra of PVC/ODA–45 and 60% AC and PVC–45 and 60% AC could not be analyzed because of the low peak resolution in the presence of high concentrations of AC.

SEM analysis

Scanning electron microscopy (SEM) images of the bottom surface (which contacts the glass during the casting process) of crosslinked and uncrosslinked HCMMMs were acquired using a scanning electron microscope. Figure 4 shows the bottom surface SEM image of a PVC–60% AC

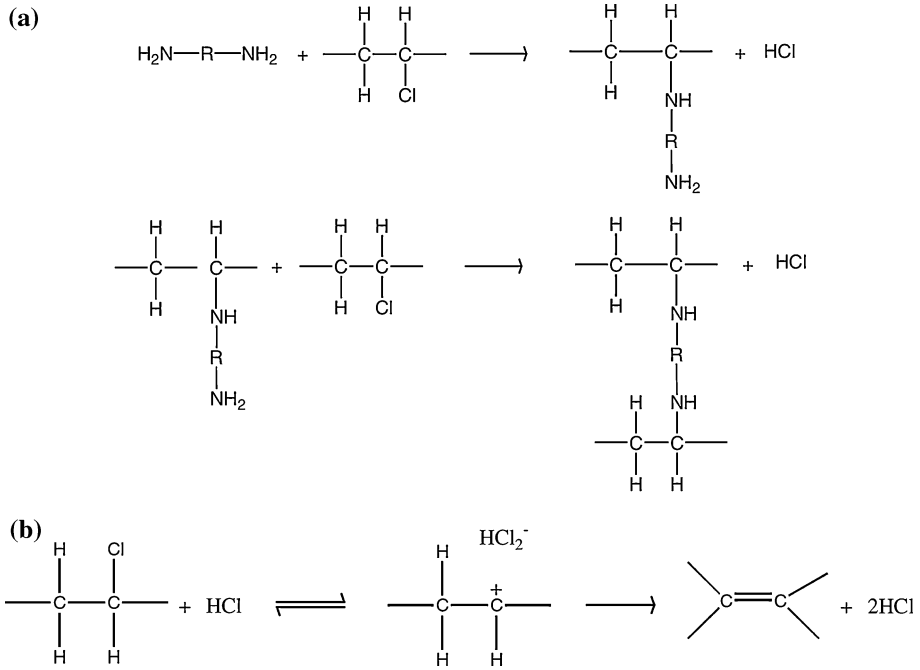

Fig. 2 **a** Crosslinking mechanism and **b** dehydrochlorination catalyzed by HCl reaction schemes from [23]

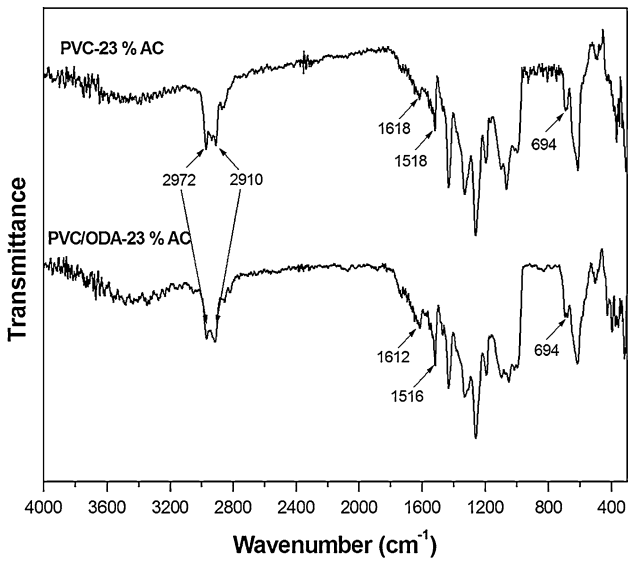

Fig. 3 FT-IR spectra of PVC–23% AC and PVC/ODA–23% AC

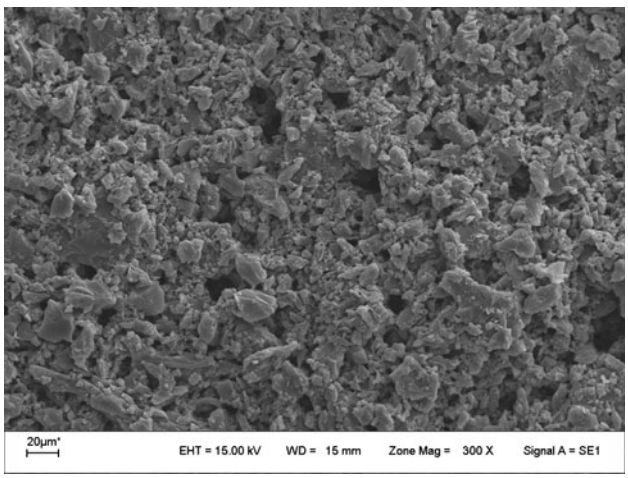

Fig. 4 SEM imaging corresponding to the bottom surface of PVC–60% AC membrane

membrane. Void spaces were visible around the carbon particles (whose diameters were ≤20 μm) indicating that the carbon particles create porous-like holes in the membrane surface. Thus, possible channel formation through the membrane could produce an increase in gas permeability, coupled with a decrease in membrane selectivity. A particle size distribution from 0.2 to 20 μm was also observed by SEM. However, structural differences between the upper and bottom surfaces were not observed in PVC–60% AC membranes.

Figure 5 shows bottom surface SEM images of a PVC/ODA–60% AC membrane. A smoother and more homogeneous porous surface was observed with a superficial hole size of ≤2 μm. In addition, PVC/ODA–60% AC membranes displayed a narrower particle size distribution, corresponding to the lowest sized carbon particles.

SEM micrographs of both crosslinked and uncroslinked HCMMMs containing 23 and 45% AC revealed structural characteristics similar to 60% AC HCMMMs. However, the crosslinking process, including the chemical reaction and the thermal treatment, favored the formation of a less permeable porous structure in all crosslinked HCMMMs.

A thin polymer layer covering the carbon particles was observed in all MMMs, indicating good contact between the polymeric and inorganic phases.

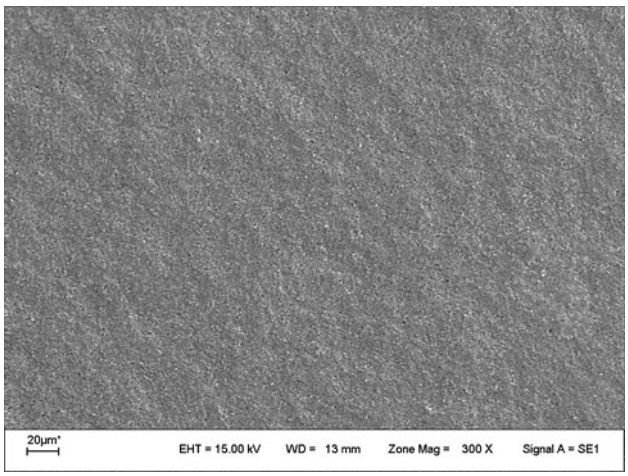

Fig. 5 SEM imaging corresponding to bottom surface of PVC/ODA–60% AC membrane

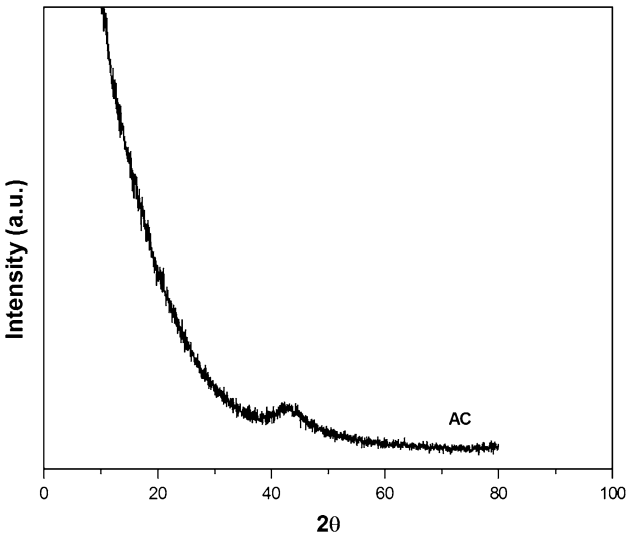

Fig. 6 X-ray diffraction of pure AC

X-ray diffraction analysis

X-ray diffraction patterns of PVC MMMs before and after crosslinking and pure AC were obtained. The effect of AC load was analysed. Figure 6 shows the diffractogram of pure AC. A single band at $2\theta = 42.3°$ (d-spacing = 2.1 Å) was observed. This band corresponds to X-ray diffractogram of graphite carbon, specifically the plane (100) of graphite. The absence of a peak at $2\theta = 24°$ (d-spacing = 3.35 Å), which corresponds to (002) plane in graphite, indicates that the Maxsorb 3000 AC presents a more graphitic nature. This observation is consistent with the ordered microporous structure of Maxsorb 3000 AC [26, 31–35]. Figure 7 shows X-ray diffractograms obtained from PVC, PVC/ODA, and PVC/ODA–23, 45, and 60% AC. Pure PVC and crosslinked PVC displayed two crystalline bands (I and II bands), laying on a wider amorphous band (A band) with lower intensity, which represents the amorphous polymer region. These results confirm the semicrystalline nature and syndiotactic arrangement of the polymeric matrix.

In addition to I, II, and A bands, PVC/ODA–AC HCMMMs presented an additional band at higher Bragg's angles, corresponding to the diffraction signal of AC (III band), in agreement with previous work [26].

Although the crosslinked MMMs also displayed a semicrystalline structure, I diffraction band in PVC/ODA and PVC/ODA–AC membranes showed a slight shift to higher Bragg's angles with respect to the pure PVC's I band, suggesting that crosslinked membranes have a lower degree of crystallinity. This reduced crystallinity may be due to: (i) restriction of the movement of polymeric chains, due to crosslinking and the presence of carbon particles; (ii) the presence of rigid aromatic rings on the crosslinker and carbon particles within polymer chains,

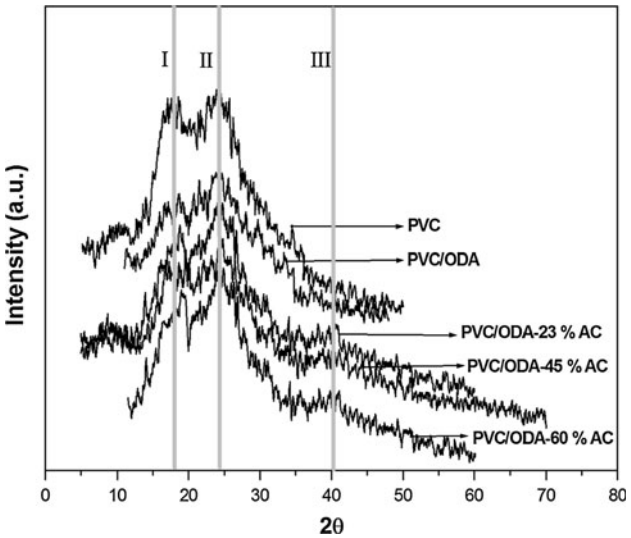

Fig. 7 X-ray diffraction of PVC, PVC/ODA, and PVC/ODA–23, 45, and 60% AC

which prevent crystalline molecular packing; (iii) loss of stereoregularity; among others. The change in the crystalline structure of PVC/ODA and crosslinked HCMMMs was also confirmed by the shift of the A band at higher Bragg's angles. Intercatenary distances (d-spacing), corresponding to I, II, III, and A bands from PVC, PVC/ODA, and PVC/ODA–AC membranes, were calculated using Eq. 1, and results are shown in Table 1. The d-spacing of uncrosslinked HCMMMs was also calculated.

PVC–AC membranes showed decreasing crystallinity with increasing carbon content. This loss of crystallinity may be due to the absence of diamine crosslinking molecules, hence the rigidification of polymeric chains around the carbon particles is more pronounced than in crosslinked MMMs, resulting in more disruption of crystalline order.

Table 1 *d*-spacing of pure polymers, HCMMMs, and the AC

Membrane	*d*-spacing (Å)			
	I band	II band	A band	AC
PVC	4.911	3.682	4.122	–
PVC/ODA	4.754	3.682	3.958	–
PVC/ODA–23% AC	4.729	3.682	3.927	2.134
PVC/ODA–45% AC	4.704	3.682	3.923	2.134
PVC/ODA–60% AC	4.679	3.682	3.919	2.134
PVC–23% AC	4.716	3.682	3.990	2.134
PVC–45% AC	–	3.531	3.458	2.134
PVC–60% AC	–	2.565	2.565	2.134

Based on X-ray analysis, carbon particles appear to act as sites of stress within the polymeric matrix, decreasing the intercatenary distances [26]. In support of this, at a carbon content of 60 wt%, polymer I and II bands converged to the A band, indicating a completely amorphous structure. Results from the above analysis are presented in Fig. 8.

Thermal properties

In order to determine the thermal resistance of HCMMMs, TGA were performed. Figure 9 shows the thermal decomposition of pure PVC and PVC/ODA. As can be seen, the first step of PVC weight loss appears at 209 °C, with a residual weight of 96%, and was completed in three steps. The last step of decomposition occurred at 576 °C, with a weight loss of 81%. Minor weight loss was observed at 124 °C, which was attributed to loss of residual solvent. For PVC/ODA, weight loss began at 162 °C, with a residual weight of 96%, and was completed in three steps.

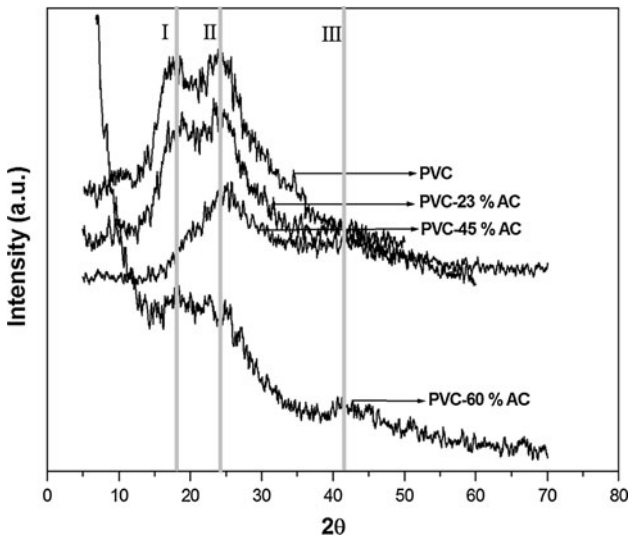

Fig. 8 X-ray diffraction of PVC and PVC–23, 45, and 60% AC

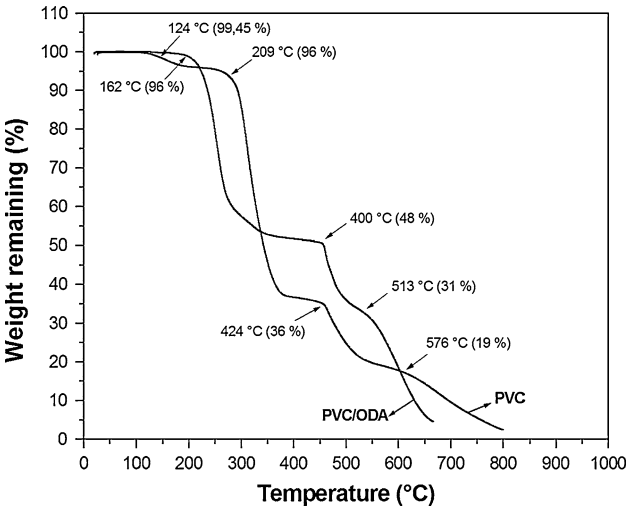

Fig. 9 TG of pure PVC and PVC/ODA

In agreement with the present study, Romero Tendero et al. [23] also reported a lower thermal resistance for crosslinked PVC than pure PVC, and found that pure PVC weight loss began at 140 °C, while crosslinked PVC decomposition began at 125 °C. The authors attributed this behavior to the presence of HCl molecules, which catalyze the degradation of crosslinked PVC.

Figure 10a, b shows thermograms corresponding to crosslinked and uncrosslinked 23 and 60% HCMMMs, respectively. As can be seen, PVC/ODA–AC and PVC–AC HCMMMs displayed less degradation steps as the carbon content increased. This was attributed to the fact that, as carbon content increases, the polymeric phase decreases, and the thermal decomposition of HCMMMs is controlled by the concentration of AC.

Despite the faster thermal decomposition of HCMMMs, the beginning step of crosslinked and uncrosslinked mixed membrane degradation appears at higher temperatures for PVC and PVC/ODA. This may be because the carbon particles cause the polymeric matrix to become more rigid, raising the initial thermal resistance of all HCMMMs. However, when the carbon content in PVC/ODA–AC and PVC–AC was 60%, both membranes displayed the same thermogram. These findings support the hypothesis that TG is controlled by AC. Thermograms of crosslinked and uncrosslinked HCMMMs with 45% AC displayed intermediate behavior, between that found for 23 and 60% AC membranes.

In order to study the effect of crosslinking and carbon content on the glassy T_g of the membranes, we conducted DSC analyses. Table 2 lists the T_g values obtained for all membranes. The T_g for pure PVC is 70 °C, indicating that at ambient temperature, the semicrystalline PVC has the mechanical and thermal properties of a flexible polymer, in agreement with its low degree of crystallinity. However,

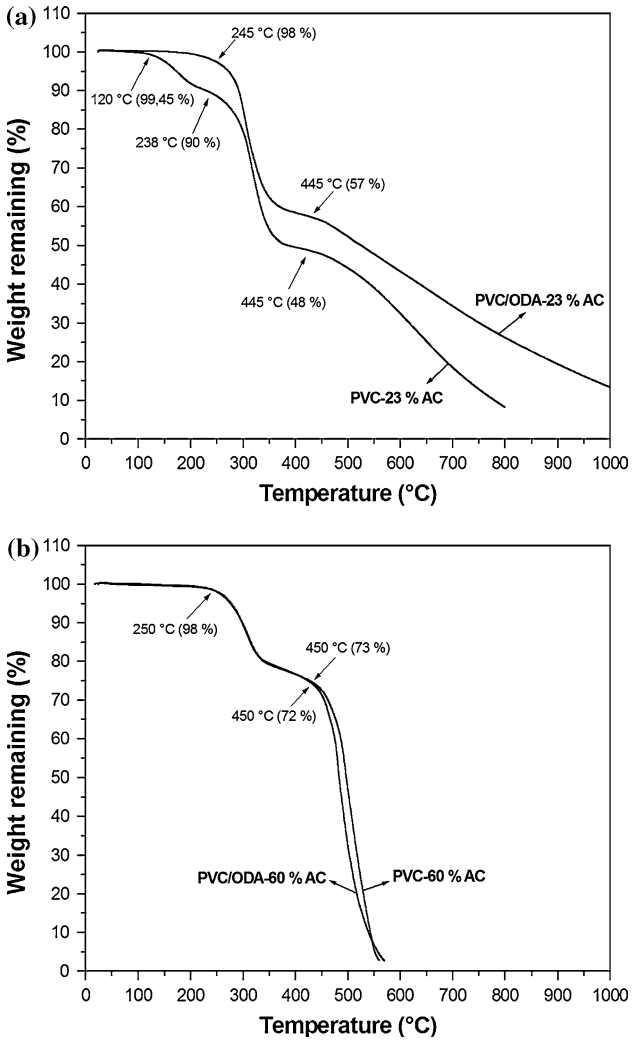

Fig. 10 TG of PVC/ODA–AC and PVC–AC **a** 23% and **b** 60%

Table 2 T_g values of membranes

Membrane	T_g (°C)
PVC	70
PVC/ODA	107
PVC/ODA–23% AC	90
PVC/ODA–45% AC	89
PVC/ODA–60% AC	89
PVC–23% AC	61
PVC–45% AC	68
PVC–60% AC	90

crosslinking the PVC with an aromatic diamine resulted in an increase in T_g to 107 °C; which was attributed to steric hindrance of the polymeric chains, not only because of crosslinking, but also because of the rigid structure of the diamine itself. This result contradicts the decreased degree of crystallinity observed for PVC/ODA versus pure PVC ("X-ray diffraction analysis" section), which might be expected to have caused a decrease in T_g. However, this apparent discrepancy may be explained by considering that movement restriction is a greater influence on T_g than crystallinity [36, 37].

Crosslinked MMMs displayed T_g values which were intermediate between those of PVC and PVC/ODA. At different AC contents, T_g values for crosslinked HCMMMs were 90 °C, indicating that loss of crystallinity plays a significant role in determining the glassy T_g for these samples. On the other hand, PVC–AC uncrosslinked membranes behaved unusually. At lower AC contents, T_g values were influenced by the degree of crystallinity; however, as carbon content increased the rigidification effect began to be dominant, increasing the T_g value up to 90 °C for 60% AC.

Gas permselectivity

Permeability was measured for all assayed gases and membranes at 35 °C ($T = 308$ K), and at a high-pressure side $p_1 = 1$ bar. Individual gases were measured in the following order: H_2, N_2, O_2, CH_4, and CO_2, to avoid probable effect of membrane plasticization in presence of CO_2 gas. Permeability coefficients determined for pure PVC and PVC/ODA membranes, and those loaded with 23, 45, and 60 wt% AC are summarized in Table 3. Permeability coefficients were obtained by averaging values from three permeation tests for each membrane. An increase in the permeability of all gases was observed with crosslinking and increasing amounts of AC.

Different gas transport mechanisms related with the membrane phase take place during the mass transfer process. Commonly, gas transport through pure polymeric membrane (PVC and PVC/ODA) occurs via a "sorption–diffusion" mechanism. According to this mechanism, gas permeation is a complex process that first involves sorption of the penetrant gas in the polymeric material, followed by diffusion of the gas molecule across the membrane matrix, due to the presence of a concentration gradient. Freeman et al. [38, 39] reported that the presence of crystalline regions in the polymeric phase was associated with decreased gas permeability, due to the insolubility of the crystalline phase to penetrant gases. In addition, movement of polymer chains in the amorphous phase is restricted by the presence of crystallites, hindering gas diffusivity through the polymeric matrix. Consistent with this, PVC/ODA showed higher gas permeability coefficients than pure PVC, in agreement with the decrease in the crystalline degree observed in the X-ray study ("X-ray diffraction analysis" section).

The high permeability coefficient values of the HCMMMs showed in Table 3 were comparable with those reported by Liang et al. [19] for carbon membranes

Table 3 Permeability coefficients of pure and HCMMMs ($T = 308$ K, $p_1 = 1$ bar)

Membrane	P_{H_2} (B) $\Delta\varepsilon \pm 4$	P_{N_2} (B) $\Delta\varepsilon \pm 7$	P_{O_2} (B) $\Delta\varepsilon \pm 6$	P_{CH_4} (B) $\Delta\varepsilon \pm 7$	P_{CO_2} (B) $\Delta\varepsilon \pm 6$
PVC	1.700	0.012	0.045	0.029	0.157
PVC/ODA	2.925	0.099	0.055	0.032	0.223
PVC/ODA–23% AC	3.277	0.230	0.291	0.276	0.728
Membrane	$\Delta\varepsilon \pm 4$	$\Delta\varepsilon \pm 4$	$\Delta\varepsilon \pm 4$	$\Delta\varepsilon \pm 4$	$\Delta\varepsilon \pm 4$
PVC/ODA–45% AC	146.24	39.58	44.13	63.03	39.18
PVC/ODA–60% AC	455.40	122.10	156.40	202.80	117.40
PVC–23% AC	1747	602.83	421.98	723.4	448.51
PVC–45% AC	197345	74248	67719	104228	71730
PVC–60% AC	650535	244279	223357	338062	234882

$[P] = 1$ Barrer (B) $= 10^{-10}$ (cm^3(STP)cm/cm^2 cmHg s); $\Delta\varepsilon$ (%) error percentage

prepared from coal tar pitch. In addition, higher gas permeabilities in uncrosslinked PVC–AC membranes than those of crosslinked PVC/ODA–AC, were in good agreement with differences observed in porous structures of HCMMMs (surface SEM imaging, "SEM analysis" section).

The increment on gas permeabilities of the MMMs with increasing carbon loading can be in part attributed to the gas flux through the pores of the carbon particles. Gas transport through porous materials can occur via various mechanisms depending on the ratio between the mean free path of the gas molecules (λ) and the pore radius (r) of the porous material. Selective transport mechanisms associated with different ratios are: molecular diffusion ($r/\lambda > 10$); Knudsen diffusion ($r/\lambda < 0.1$); series resistance (molecular-Knudsen diffusion) ($0.1 < r/\lambda < 10$). Other selective flux mechanisms can take place through porous materials, among them: surface diffusion; capillary condensation; and molecular sieving.

The mean free path of gas molecule can be calculated from the simplified kinetic theory of dilute gases [40, 41]:

$$\lambda_i = \frac{kT}{\sqrt{2}\pi\sigma_i^2 p} \tag{4}$$

where k is the Boltzman constant $= 1{,}38 \times 10^{-16}$ (erg K^{-1}); σ_i collision diameter of molecule i; and p the gas pressure. The characteristic physical parameters of gases, λ and r/λ values at $T = 308$ K, $p = 1$ bar, and $r = 10.85$ Å (from "Materials and methods" section) are shown in Table 4.

The r/λ values clearly indicate Knudsen diffusion should be the main gas transport mechanism through the carbon porous media ($r/\lambda \ll 0.1$). During Knudsen diffusion, gas transport takes place along a large pore, where the probability of molecule-pore wall collision is higher than molecule–molecule collision. In this case, the Knudsen permeability, P_i^K, can be expressed by [42, 43]:

$$P_i^K = \frac{D_{ii}^K}{R_g T}\frac{\varepsilon}{\tau} \tag{5}$$

where R_g is the universal gas constant; ε and τ the porosity and tortuosity of the porous media; and D_{ii}^K the Knudsen diffusion coefficient of the gas in a cylindrical pore, given by [40, 41]:

$$D_{ii}^K = \frac{2}{3} r \left(\frac{8R_g T}{\pi M_i}\right)^{1/2} \tag{6}$$

where M_i is the gas molecular weight.

Furthermore, high amount of carbon could induce formation of microporous cavities and channelling at the inorganic–polymeric interface. In this case, high gas transport through the interface cavities due to non-selective viscous flow lead to low improvement in the mixed

Table 4 Gas characteristic parameters ($T = 308$ K, $p_1 = 1$ bar)

Gas	M (g/gmol)	σ (Å)	λ (Å)	$(r/\lambda) \times 10^2$	Ω_μ	$\mu \times 10^4$ (g cm^{-1} s^{-1})
H_2	2.016	2.915	1111.0	0.977	0.852	0.919
N_2	28.020	3.681	697.0	1.558	1.009	1.813
O_2	32.000	3.433	801.3	1.355	1.066	2.109
CH_4	16.040	3.822	646.5	1.680	1.130	1.136
CO_2	44.010	3.996	591.4	1.836	1.273	1.529

Table 5 Ideal separation factors ($T = 308$ K, $p_1 = 1$ bar.)

Membrane	α_{H_2/CH_4} $\Delta\varepsilon \pm 11$	α_{H_2/CO_2} $\Delta\varepsilon \pm 10$	α_{H_2/CO_2} $\Delta\varepsilon \pm 10$	α_{H_2/N_2} $\Delta\varepsilon \pm 11$	α_{CO_2/CH_4} $\Delta\varepsilon \pm 13$
PVC	59.44	10.83	37.53	144.07	5.49
PVC/ODA	92.56	13.12	53.09	29.58	7.06
PVC/ODA–23% AC	11.87	4.50	11.26	14.28	2.64
Membrane	$\Delta\varepsilon \pm 8$	$\Delta\varepsilon \pm 8$	$\Delta\varepsilon \pm 8$	$\Delta\varepsilon \pm 8$	$\Delta\varepsilon \pm 8$
PVC/ODA–45% AC	2.32	3.73	3.31	3.69	0.62
PVC/ODA–60% AC	2.25	3.88	2.91	3.73	0.58
PVC–23% AC	2.42	3.90	4.14	2.90	0.62
PVC–45% AC	1.89	2.75	2.91	2.66	0.69
PVC–60% AC	1.92	2.77	2.91	2.66	0.69

$\Delta\varepsilon$ (%) error percentage

membrane selectivity. The viscous flow permeability through a porous media, P_i^V, can be expressed as [42, 43]:

$$P_i^V = \frac{r^2\varepsilon}{8\tau\mu_i}\frac{p}{R_g T} \tag{7}$$

where μ_i is the gas viscosity.

To discuss the flux mechanisms contribution on the total gas mass transport through the membranes, the selectivity factor was taken as reference parameter. To analyze membrane permselectivity, H_2/CH_4, H_2/CO_2, H_2/O_2, H_2/N_2, and CO_2/CH_4 systems were chosen, because of their importance for commercial and for purification uses. Ideal separation factors of these systems evaluated from Eq. 3 are shown in Table 5.

In Table 6 are summarized the Knudsen ideal separation factors ($\alpha_{i/j}^K$) and the ideal viscous flow ratio ($\phi_{i/j}^V$) under the same experimental conditions of T and p. These parameters were obtained from Eqs. 5–7 as follows:

$$\alpha_{i/j}^K = \frac{P_i^K}{P_j^K} = \frac{D_{ii}^K}{D_{jj}^K} = \sqrt{\frac{M_j}{M_i}} \tag{8}$$

$$\phi_{i/j}^V = \frac{P_i^V}{P_j^V} = \frac{\mu_j}{\mu_i} = \sqrt{\frac{M_j}{M_i}}\frac{\sigma_i^2\Omega_{\mu i}}{\sigma_j^2\Omega_{\mu j}} \tag{9}$$

where the pure gas viscosities at low density were evaluated from the Chapman–Enskog equation [40]:

$$\mu_i(\mathrm{g\,cm^{-1}\,s^{-1}}) = 2,6693 \times 10^{-5}\frac{\sqrt{M_i T}}{\sigma_i^2\Omega_{\mu i}} \tag{10}$$

Table 6 Knudsen separation factor and viscous flow ratio ($T = 308$ K, $p_1 = 1$ bar)

	H_2/CH_4	H_2/CO_2	H_2/O_2	H_2/N_2	CO_2/CH_4
$\alpha_{i/j}^K$	2.82	4.67	3.98	3.73	0.60
$\phi_{i/j}^V$	1.24	1.66	2.30	1.97	0.74

being $\Omega\mu_i$ the collision integral.

Representative effects of AC content in HCMMMs on the ideal separation factor for H_2/CH_4 and H_2/O_2 systems are shown in Fig. 11a, b. For comparison, the Knudsen separation factor and viscous flow ratio were included in figures. As expected, PVC and PVC/ODA polymeric membranes (AC% = 0) displayed the highest separation factors (the lowest gas permeabilities) which follow a "sorption–diffusion" selective mechanism. PVC/ODA–45 and 60% AC and PVC–23–45 and 60% AC, presented ideal separation factor values near to those of Knudsen selectivities indicating the total gas flux through the membrane was mainly controlled by the Knudsen mechanism being the sorption diffusion mechanism negligible. The deviation of separation factors from Knudsen selectivity to viscous flow ratio can be attributed to the presence of channels and/or defects in both the carbon interparticles and polymer–carbon interface. When the AC content in the crosslinked PVC–ODA was 23%, the selectivities were between those of pure polymers and porous Knudsen diffusion suggesting that permeate flux was controlled by both the sorption–diffusion and Knudsen mechanisms. A similar selectivity behavior from other gas systems (H_2/CO_2, H_2/N_2, and CO_2/CH_4) was observed.

As can be seen, both crosslinked and uncroslinked HCMMMs containing 45 and 60% AC are attractive membranes for industrial applications, because of their high gas permeabilities, which are comparable with those of pyrolytic carbon membranes [19].

Conclusions

A semicrystalline polymer was used to prepare MMMs containing increasing amounts of AC (the highest reported to date) in order to obtain highly permeable MMMs similar

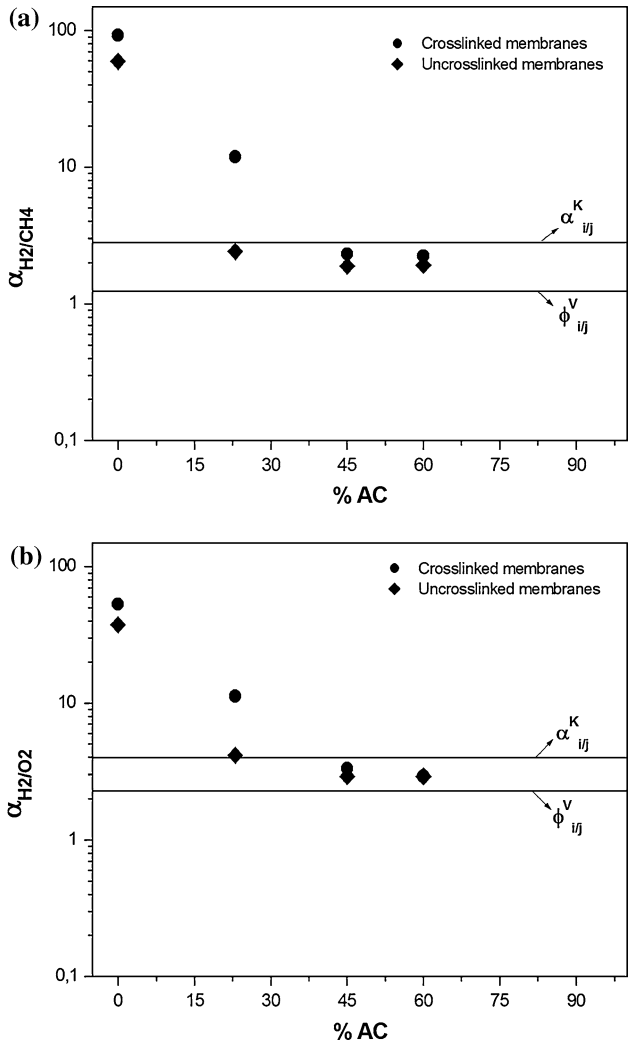

Fig. 11 Effects of AC content in HCMMMs on the ideal separation factors for **a** H_2/CH_4 and **b** H_2/O_2

to carbon membranes. In fact, the gas permeation properties of the HCMMMs with good processability were evaluated and the results were comparable with carbon membranes. FT-IR enabled verification of the presence of crosslinking, and determination of the mechanism of the crosslinking reaction. SEM imaging and X-ray diffraction analysis enabled elucidation of the structure of the HCMMMs. Based on these analyses; we observed that as the carbon load increases, the inorganic particles are able to form channels and/or defects in both the carbon interparticles and polymer–carbon interface. From X-ray diffraction patterns, we observed that at the highest carbon content, the lowest polymer crystalline degree was observed, and this effect was more pronounced in the absence of crosslinking. Crosslinking the polymeric matrix and increasing the AC content the T_g of HCMMMs is raised. TGA revealed faster TG for all HCMMMs with respect to pure and crosslinked PVC. However, a higher initial degradation temperature for all HCMMMs was observed indicating better thermal resistance with respect to pure polymers. Pure PVC and PVC/ODA showed a selective diffusion mechanism, while PVC/ODA–23% AC presented an intermediate selective mechanism between those of polymer matrix and porous structure. Crosslinked and uncrosslinked HCMMMs with high AC amount (45–60 wt%) are attractive membranes because of their high gas permeabilities, which are comparable with those of pyrolytic carbon membrane; nevertheless, their selectivity values are near to the ideal Knudsen separation factor.

References

1. Saufi SM, Ismail AF (2004) Carbon 42:241
2. Fuertes AB, Centeno TA (1998) J Membr Sci 144:105
3. Kyotani T (2000) Carbon 38:269
4. Kärger J, Ruthven DM (1992) Diffusion in zeolites and other microporous solids. Wiley/Interscience, New York
5. Breck DW (1974) Zeolite molecular sieves: structure, chemistry, and use. Wiley/Interscience, New York
6. Stern SA (1994) J Membr Sci 94:1
7. Vu DQ, Koros WJ, Miller SJ (2003) J Membr Sci 211:311
8. Koros WJ, Mahajan R (2000) J Membr Sci 175:181
9. Koros WJ, Fleming GK (1993) J Membr Sci 83:1
10. Koros WJ, Coleman MR, Walker DRB (1992) Annu Rev Mater Sci 22:47
11. Zhang Y, Musselman IH, Ferraris JP, Balkus KJ Jr (2008) Ind Eng Chem Res 47:2794
12. Romero AI, Parentis ML, Habert AC, Gonzo EE (2011) J Mater Sci 46:4701. doi:10.1007/s10853-011-5380-4
13. Mahajan R, Koros WJ (2000) Ind Eng Chem Res 39:2692
14. Marchese J, Garis E, Anson M, Ochoa NA, Pagliero C (2004) J Membr Sci 243:19
15. Marchese J, Anson M, Ochoa NA, Prádanos P, Palacio L, Hernández A (2006) Chem Eng Sci 61:5448
16. Ismail AF, David LIB (2001) J Membr Sci 193:1
17. Hsieh HP (1990) Membr Mater Proc 84:1
18. Hosseini SS, Chung TS (2009) J Membr Sci 328:174
19. Liang C, Sha G, Guo S (1999) Carbon 37:1391
20. Ash R, Barrer RM, Lowson RT (1973) J Chem Soc Faraday Trans I 69:2166
21. Fuertes AB (2000) J Membr Sci 177:9
22. Petersen J, Matsuda M, Haraya K (1997) J Membr Sci 131:85
23. Romero Tendero PM, Jimenez A, Greco A, Maffezzoli A (2006) Eur Polym J 42:961
24. Han SP, Park KJ, Lee K (2002) J Appl Polym Sci 83:1947
25. Bao YZ, Weng ZX, Ming Z, Pan ZR (2000) J Appl Polym Sci 76:868
26. García MG, Marchese J, Ochoa NA (2010) J Appl Polym Sci 118:2417
27. Beltrán M, García JC, Marcilla A (1997) Eur Polym J 33:453
28. Beltrán M, Marcilla A (1997) Eur Polym J 33:1135
29. Matuana LM, Woodhams RT, Balatinecz JJ, Park CB (1998) Polym Compos 19:446
30. Starnes WH Jr (2002) Prog Polym Sci 27:2133
31. Steel KM, Koros WJ (2003) Carbon 41:253
32. Zhu ZL, Li AM, Yan L, Liu FQ, Zhang QX (2007) J Colloid Interface Sci 316:628

33. Carrott PJM, Nabais JMV, Ribeiro Carrott MML, Pajares JA (2001) Carbon 39:1543
34. Yang H, Gong MC, Chen YQ (2011) J Nat Gas Chem 20:460
35. Lee JJ, Suh JK, Hong JS, Lee JM, Lee YS, Park JW (2008) Carbon 46:1648
36. Sperling LH (2006) Introduction to physical polymer science, 4th edn. Wiley, New York
37. International ASM (2003) Characterization and failure analysis of plastics, 1st edn. The Materials Information Society, New York
38. Lin H, Van Wagner E, Swinnea JS, Freeman BD, Pas SJ, Hill AJ et al (2006) J Membr Sci 276:145
39. Sunderrajan S, Freeman BD, Hall CK, Pinnau I (2001) J Membr Sci 182:1
40. Bird RB, Stewart WE (2008) In: Lightfoot EN (ed) Transport phenomena, 2nd edn. Reverté S.A, México, ISBN 968-6708-17-0
41. Curtiss CF, Bird RB (1954) In: Hirschfelder JO (ed) The molecular theory of gases and liquids, 1st edn. Wiley, New York
42. Anson M (2009) Synthesis of composite mixed matrix membranes for CO_2-CH_4 separation. Thesis doctoral, UNSL, San Luis
43. García MG (2011) Synthesis of polyimides and membrane preparation to be applied to the H_2 separation. Thesis doctoral, UNSL, San Luis